How accurately can we model magma reservoir failure with uncertainties in host-rock rheology?

Y. Zhan[1] and P. M. Gregg[1]

[1]*Department of Geology, University of Illinois - Urbana-Champaign, Urbana, Illinois, USA*

Corresponding author: Yan Zhan (yanzhan3@illinois.edu)

Key points:

- Predictions of the onset magma chamber failure are more sensitive to Young's modulus than other elastic properties
- Displacement at the onset of magma reservoir failure is not sensitive to variations in Young's modulus for stiff host rocks (E>40 GPa)
- Whether viscosity affects brittle failure depends on host-rock relaxation time scales

Abstract

Forecasting the onset of a volcanic eruption from a closed system requires understanding its stress state and failure potential, which can be investigated through numerical modeling. However, the lack of constraints on model parameters, especially rheology, may substantially impair the accuracy of failure forecasts. Therefore, it is essential to know whether large variations and uncertainties in rock properties will preclude the ability of models to predict reservoir failure. A series of 2-dimensional, axisymmetric models are used to investigate sensitivities of brittle failure initiation to assumed rock properties. The numerical experiments indicate that the deformation and overpressure at failure onset simulated by elastic models will be much lower than the viscoelastic models, when the timescale of pressurization exceeds the viscoelastic relaxation time of the host-rock. Poisson's ratio and internal friction angle have much less effect on failure forecasts than Young's modulus. Variations in Young's modulus significantly affect the prediction of surface deformation before failure onset when Young's modulus is <40 GPa. Longer precursory volcano-tectonic events may occur in weak host-rock (E <40 GPa) due to well-developed Coulomb failure prior to dike propagation. Thus, combining surface deformation with seismicity may enhance the accuracy of eruption forecast in these situations. Compared to large and oblate magma systems, small and prolate systems create far less surface-uplift prior to failure initiation, suggesting more frequent measurements are necessary.

1 Introduction

Ground deformation is one of the most widely used methods to evaluate and forecast volcanic unrest (Sparks, 2003). Geodetic monitoring methods, including Global Navigation Satellite System (GNSS) and Interferometric Synthetic Aperture Radar (InSAR) provide temporal surface deformation observations of active volcanoes and a glimpse into the evolution of the underlying magmatic system. Geodetic data alone cannot uniquely constrain some important parameters of magma reservoirs, like size or overpressure (e.g., Segall, 2019). The architecture and evolution of a magma reservoir may be better interpreted by combining multiple geophysical observations, such as seismology, gravity, and magnetotellurics. However, a good knowledge of reservoir geometry and deformation history does not ensure an accurate eruption forecast. Substantial surface inflation may not indicate the propensity of volcano eruption (e.g., Biggs et al., 2014; Biggs & Pritchard, 2017).

Numerical volcano models provide important evaluations of ground deformation signals using stress calculations and failure predictions, which are essential to give insight into the dynamic evolution of magma systems (e.g., Grosfils, 2007; Albino et al., 2010; Gerbault et al., 2012, 2018; Gregg et al., 2012, 2013; Hickey & Gottsmann, 2014; Hickey et al., 2015). Furthermore, the recent development of sequential data assimilation approaches provides near real-time estimates of overpressure and stress state of magmatic systems, which is a promising step towards forecasting volcanic unrest with advanced observations (e.g., Gregg & Pettijohn, 2016; Bato et al., 2017, 2018; Zhan & Gregg, 2017; Zhan et al., 2017; Gregg et al., 2018; Albright et al., 2019). However, before an accurate forecast can be conducted, we need to understand the sensitivity of model results to different model parameters in a magmatic system, such as geometry, initial stress state, and rock properties. Among them, the effect of chamber geometry has been systematically studied by previous investigations (e.g., Mogi, 1958; Yang et al., 1988; Segall, 2019), and the initial stress is controlled by many factors such as the deformation history and tectonics, which is beyond the scope of this paper. We focus our current effort on evaluating the impact of rock rheology, which is an important factor in magma system models, and is not well constrained.

Rock properties for different volcanoes can be distinct. For example, the Young's modulus inferred by static loading is no more than 1 GPa for Merapi volcano (Beauducel et al., 2000), while the Young's modulus is greater than 40 GPa for volcanoes in Iceland (Grapenthin et al., 2006). Even for one volcano, rock properties inferred by different approaches may not be consistent. Dynamic Young's modulus calculated using seismic methods can be significantly higher than static Young's modulus determined by laboratory rock tests and geodetic modeling. For example, dynamic Young's modulus of the crust in Mt. Etna inferred by P-wave velocity can reach 100 GPa (e.g., Currenti et al., 2007), while laboratory rock tests show that Young's modulus of a basaltic samples from Mt. Etna is < 30 GPa (Heap et al., 2010). Additionally, Young's modulus and Poisson's ratio can be modified by ~30% during repeating loading and unloading (Heap et al., 2010). Similarly, the viscosity of the crust varies from 10^{15} to 10^{21} $Pa \cdot s$ depending on the composition and temperature (e.g., Newman et al., 2001). Considering that a systematic discussion on the effects of rock property on modeling is still absent, this study aims to test the effect of varying rock properties on modeling brittle failure around a magma reservoir.

In this paper, we conduct a series of sensitivity tests using 2-dimensional, axisymmetric models to evaluate the impact of the uncertainties in assumed rheological parameters. First, we use viscoelastic models to evaluate the sensitivities of Critical Maximum Surface Uplift (CMSU) and overpressure before brittle failure onset to a variety of rheological parameters, such as viscosity, Young's modulus, and loading rate. Then, a series of elastic models are used to test the effects of Young's modulus, Poisson's ratio, internal friction angle, and tensile strength on the CMSU and critical overpressure. The effects of these parameters are evaluated under different geometrical conditions including depth, size, and shape of the magma body. Of particular interest in this investigation is whether large variations and uncertainties preclude the ability of models to predict failure of a magma reservoir. Here we only consider the homogenous rock property to quantify the uncertainties from the varying values of rock properties. Heterogeneity in those properties is also important (e.g., De Natale & Pingue, 1996; Masterlark, 2007) and should be studied systematically in the future.

2 Methods

2.1 Model setup

We use 2-dimensional, axisymmetric models (Fig. 1a) solved by finite element code COMSOL Multiphysics 5.3 to simulate the surface deformation and failure of the host-rock due to an inflating magma body with an applied overpressure (OP; e.g., Gregg at al., 2012, 2013). Overpressure is assumed along the boundary of the magma body as a force in excesses of the lithostatic stress. Roller boundary conditions are defined at the side and bottom of the model. Gravity is loaded as a body force, which is balanced by an initial hydrostatic stress (i.e., $\sigma_1 = \sigma_2 = \sigma_3 = \rho g z$) prior to the addition of overpressure along the boundary of the spheroid (Fig. 1a).

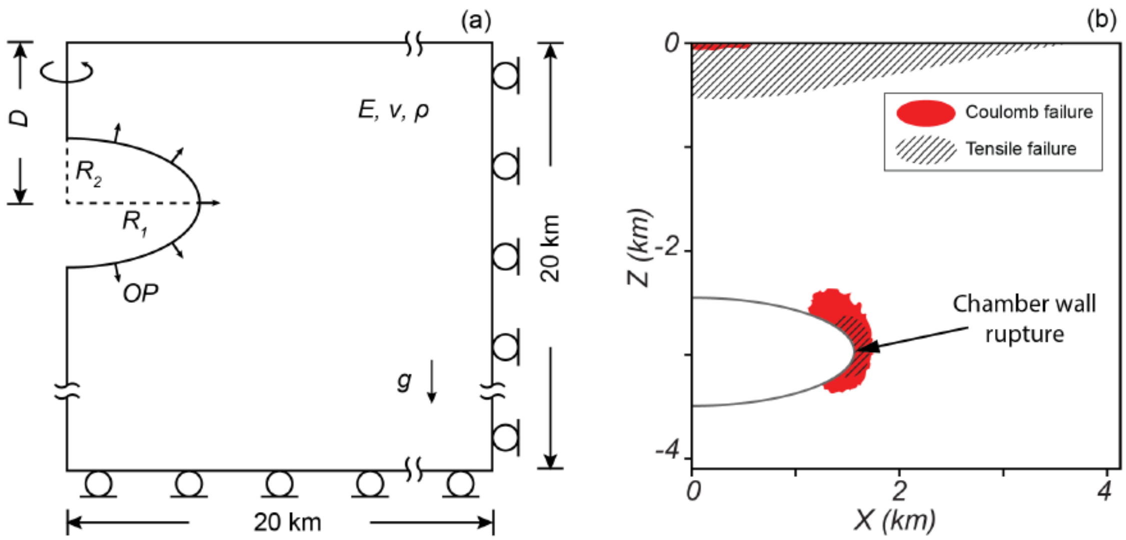

Figure 1. Model setup and failure onset. (a) The 2-dimensional axial symmetric model (20 x 20 km). The left boundary is the axis of symmetry. The right and bottom boundaries are defined as roller-type boundary condition. The magma body is represented by an elliptical void along which an overpressure (OP = pressure in excess of the lithostatic pressure) boundary condition is applied. The mesh size of the model ranges from ~100 m around the chamber to ~1000 m near the right and bottom edges. (b) The failure distribution for a model with a Young's modulus of 50 GPa when the surface uplift is 3 m. The Critical Maximum Surface Uplift (CMSU) is the calucated uplift when the chamber wall rupture is initiated, and is much lower than 3 m. The shaded red area indicates Coulomb failure, while the hatched region indicates tensile failure.

2.2 Rupture of the magma chamber

We use the Coulomb failure criterion (Eq. 1) and the tensile failure criterion (Eq. 2) to calculate failure in the host rocks due to overpressure loading. Coulomb failure or tensile failure is triggered, when:

$$\frac{\sigma_{\_} / \sigma_0}{2}\cos\phi - \frac{\sigma_{\_}\, 6\, \sigma_0}{2}\tan\phi - C_0 > 0 \quad (1)$$

or

$$-\sigma_3 - T_0 > 0, \quad (2)$$

where ϕ is the internal friction angle, C_0 and T_0 are the rock's cohesion and tensile strength, and σ_1 and σ_3 are maximum and minimum principal stresses (Table 1).

Table 1. Model variables and parameters

Name	Description
D	Depth to the center of the magma chamber (-1, -3, -5, -9 km)
R_1	Half-width of the chamber (variable; km)
R_2	Half-height of the chamber (variable; km)
OP	Overpressure - pressure excess the lithostatic pressure (variable; MPa)
d(OP)/dt	Overpressure loading rate for viscous tests

	$25 \times 10^{1}, 5 \times 10^{0}, 5 \times 10^{/1}, 5 \times 10^{/2}, 5 \times 10^{/3}, 5 \times 10^{/4}\ MPa/day3$
η	Viscosity ($2\times 10^{15}, 2 \times 10^{17}, 2 \times 10^{19}, 2 \times 10^{21}\ Pa \cdot s$)
E	Young's Modulus (5, 20, 40, 60, 80 GPa)
v	Poisson's ratio (0.15, 0.25, 0.35)
ρ	Density of the host-rock (2700 kg/m^3)
g	Gravitational acceleration (9.8 m/s^2)
C_0	Cohesion of the host-rock (E / 1000; MPa)
T_0	Tensile strength of the host-rock (C_0 / 2.5; MPa)
φ	Internal friction angle of the host-rock (15° ~ 35°)
σ_1	Maximum principal stress (variable; MPa)
σ_3	Minimum principal stress (variable; MPa)
CMSU	Critical maximum surface uplift (variable; m)

Previous rock experiments have shown a uniform, linear relationship between uniaxial compressive strength (UCS) and Young's modulus for worldwide andesites, basalt, tuff, and sandstone (e.g., $UCS = 2.28 + 4.11\ E$ by Bradford et al., 1998; $UCS = 1.65 + 5.88\ E$ by Dinçer et al., 2004). The uniaxial compressive strength is further defined by Hoek (1990) as:

$$UCS = \frac{2C_0 \cos\phi}{21/\ \sin\phi 3}. \quad (3)$$

Therefore, the cohesion of the rock is a linear function of Young's modulus at any given internal friction angle. The internal friction angle of the rock ranges from 15° to 35° (Byerlee, 1978). Combining the empirical equation of UCS (Braford et al., 1998; Dinçer et al., 2004) and Equation (3), we can express the cohesion of rock as a function of Young's modulus (Fig. S1a). The relationship between cohesion and Young's modulus using different empirical equations and friction is in the same order (Fig. S1a). We use the empirical equation by Bradford et al. (1998) and the friction angle as 35° assuming rock cohesion:

$$C_0 = E \times 10^{/3}. \quad (4)$$

The tensile strength of the rock is usually 1/10 of its UCS (e.g., Jaeger et al., 2007). Therefore, we assume the tensile strength is approximately given by (Fig. S1b)

$$T_0 = E \times 0.4 \times 10^{/3}, \quad (5)$$

where E is the Young's modulus applied in the model. When a magma chamber is inflating, failure tends to initiate at (1) the vertex of an oblate spheroid, and (2) near the surface of the model space above the magma chamber (Fig. S2). Then, the failure region expands and connects to form through-going failure (Fig. S2). This stage is highly path-dependent, which means the distribution of previous failure and weakness will impact generation of new fractures. Additionally, the propagation of fractures may accommodate the transport of magma if the stresses are properly oriented (i.e., dike propagation coinciding with mode-I failure). The predicted overpressure at which the through-going failure has formed (Fig. S2) may be greatly overestimated, if the accumulated damage in host-rocks is not taken into consideration. In this study, we focus on failure initiated along the magma chamber, representing chamber rupture (Fig. 1b). We calculate the overpressure and the maximum surface uplift (i.e., the maximum vertical surface displacement directly above the source center) of a volcano at its initial rupture as a function of the Critical Maximum Surface Uplift (CMSU). Brittle failure of rock is generally thought to trigger high-frequency or "volcano- tectonic" (VT) earthquakes (e.g., Roman and

Cashman, 2006). In practice, CMSU can infer how much precursory deformation can be observed before the onset of VT earthquakes.

2.3 Calculation of CMSU and critical overpressure

The viscous effect is tested by a series of viscoelastic models which employ a standard linear solid rheology (after Del Negro et al., 2009). In the viscoelastic tests, viscosity varies from 10^{15} to 10^{21} $Pa \cdot s$ (Newman et al., 2001) and different overpressure loading rates are assumed from 50 MPa per day to 50 MPa per 100,000 days representing unrest episodes from single-day-scale to hundred-year-scale (Table 1). Each viscous model is loaded by a constant overpressure rate from an equilibrium stress state. The loading process has been evenly divided into 50 steps until the overpressure reaches 50 MPa. We choose 50 MPa as a terminal overpressure to ensure the failure occurrence. Using Eq. 1 and 2, we can determine at which step failure has been initiated along the chamber wall. Therefore, the overpressure and CMSU at that step are the critical overpressure and CMSU. The viscous tests aim to show whether and when host rock viscosity will impact failure initiation.

In the elastic tests, the Young's modulus varies from 5 GPa to 80 GPa, covering the range in uncertainty for upper crustal rocks (e.g., Aggistalis et al., 1996; Dinçer et al., 2004). Although a significantly low Young's modulus (E<1 GPa) has been observed at Merapi volcano (e.g., Beauducel et al., 2000), it may present the effect of an unconsolidated edifice material, which is too low to represent the average upper crust. We also test three Poisson's ratios from 0.15 to 0.35 (Christensen, 1996; Gercek, 2007) and three internal friction angles from 15° to 35° (Byerlee, 1978). The parameters and variables used in the models are shown in Table 1. For elastic tests, we use an approach method to calculate the CMSU and critical overpressure. First, we model the stress field with an initial overpressure (i.e., 50 MPa, but not important). Then, we calculate residual strengths along the chamber wall, which are defined by the left-hand sides (LHS) of Eq. 1 and 2. In the next iteration, we either increase or decrease the overpressure to reduce the residual. We iterate this process until absolute residual strength of any point along the chamber wall is < 5% of the rock cohesion or tensile strength. It usually takes less than 10 iterations to approach the critical overpressure and CMSU at failure onset. In all tests, the critical overpressure and CMSU for both tensile and Coulomb failure are calculated to determine which type failure occurs first.

All models are assumed to be homogeneous and isotropic to simplify the calculation. More sophisticated models with temperature dependent rheology and pre-existing features will be tested in future investigations. However, this simple approach is capable of providing a meaningful evaluation of when uncertainties in elastic moduli overwhelm a model's ability to predict the failure of a magmatic system.

3 Results

3.1 The viscous effect

We calculate the Critical Maximum Surface Uplift (CMSU) prior to the presence of the initial tensile or Coulomb failure for the models with different viscosities and Young's moduli (Fig. S3 and S4). Since the loading rate is important in viscoelastic models, we test rates from 50

MPa / day to 50 MPa / 100,000 day to mimic a wide range of replenishment rates for magma chambers. In general, when the loading rate is low enough, the CMSUs calculated by the viscoelastic models start to deviate from the elastic models. Higher CMSUs are expected in viscous models compared to elastic models, if the characteristic time of loading (i.e., the time-span for the chamber to be pressurized to 50 MPa) is larger than the viscoelastic relaxation time (Fig. S3). Models with higher viscosity ($\eta > 10^{19}$ $Pa \cdot s$) tend to behave elastically creating the same CMSU as the elastic model even if the loading rate is as low as 50 MPa per 10 years (Fig. S3). We argue that the viscous effect can be neglected if the CMSU prior to failure calculated by a viscoelastic model equals the elastic model with the same elastic moduli (Fig. S3). The deviation of the CMSU by a viscoelastic model from an elastic model is controlled by the relaxation time of host-rock and the characteristic time of loading (Fig. 2). When the characteristic time is significantly longer than the relaxation time of the model, the viscous effect cannot be neglected (Fig. 2). A rock with lower Young's modulus or higher viscosity has a longer relaxation time, which is more likely to behave elastically under the same loading rate. Both viscoelastic and elastic models predict the same critical overpressure prior to failure onset at a given Young's modulus, indicating that the overpressure is independent of the viscosity and loading rate (Fig. S4). The critical overpressure is only controlled by the Young's modulus and rock strength.

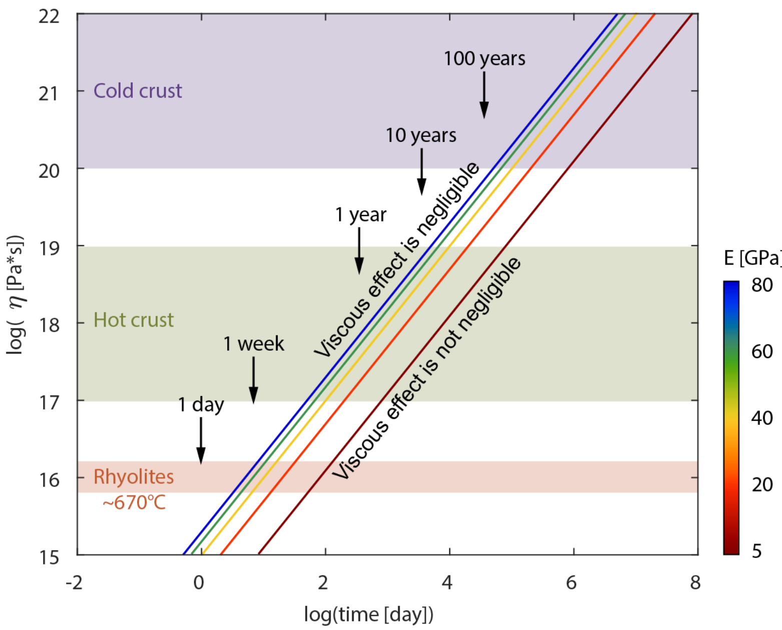

Figure 2. The relaxation times for the viscoelastic models. If the time span of pressurization prior to rupture of the magma chamber's wall is shorter than the relaxation time, the viscous effect can be neglected. The Critical Maximum Surface Deformation (CMSU; Fig. S3) calculated by a viscoelastic model is larger than the CMSU calculated by an elastic model with the same Young's modulus. The viscosity of the crust at different conditions are taken from Newman et al. (2001).

3.2 Elastic properties

According to the viscoelastic tests, a linear elastic model is appropriate in cases when the loading time span from zero overpressure to reservoir failure is shorter than the relaxation time (i.e., high loading rate, > 50 MPa / 10 year). Therefore, in these conditions, the elastic moduli and brittle failure parameters become critical for forecasting failure onset. To further examine the effects of other rock properties, we conduct a series of elastic tests on Young's modulus, rock strength which is determined by Young's modulus, Poisson's ratio, and internal friction angle. In particular, the depth, radius, and aspect ratio of the chamber are varied to provide a broad view of the failure predictions (Table 2; Fig. S5).

Table 2. Geometric parameters and model notation

Model No.	***Depth-to-center D (km)***	***Half-width R_1 (km)***	***Aspect ratio R_1/R_2***
Viscous Test	-3	1.5	3
Elastic Elastic Test 1 (Depth)			
Dp1	-1	1.5	3
Dp2	-3	1.5	3
Dp3	-5	1.5	3
Dp4	-7	1.5	3
Dp5	-9	1.5	3
Elastic Elastic Test 2 (Size)			
Rd1	-3	0.5	3
Rd2	-3	1.0	3
Rd3	-3	1.5	3
Rd4	-3	2.0	3
Rd5	-3	2.5	3
Elastic Elastic Test 3 (Depth + Size)			
DR1	-1	0.74	3
DR2	-2	1.15	3
DR3	-3	1.50	3
DR4	-4	1.81	3
DR5	-5	2.09	3
Elastic Elastic Test 4 (Aspect Ratio)			
L1	-3	1.04	1
L2	-3	1.31	2
L3	-3	1.50	3
L4	-3	1.65	4
L5	-3	1.78	5

H2	-3	0.83	1/2
H3	-3	0.72	1/3
H4	-3	0.66	1/4

Geodetic data recording the pattern of surface deformation can constrain depth and aspect ratio of the magma chamber. For example, a deeper chamber exhibits a longer wavelength signal (Fig. S5a) as illustrated elegantly by the Mogi (1958) model. The horizontal displacement is more sensitive to the aspect ratio (e.g., Dieterich and Decker, 1975; Yang et al., 1988; Fig. S5d), the vertical displacement patterns of the models with different aspect ratios are similar. Parameters like radius or total volume of the chamber cannot be constrained by the deformation patterns alone (Fig. S5b).

Given the same size and shape of a chamber (Elastic Test 1), deeper magma bodies generate lower CMSU before failure onset than shallower magma bodies (Fig. 3a). Although a deeper chamber requires a higher overpressure to fail due to the more substantial confining pressure (Fig. 3b), the higher overpressure generates less detectable surface deformation. Deeper chambers also have a smaller range of CMSU for different Young's moduli. The range of CMSU for a chamber below 7 km is less than 0.3 m, even if Young's modulus of crust varies from 20 GPa to 80 GPa, indicating that variation in Young's modulus has a less of an effect on the accuracy of the failure forecast. Similar to the depth-dependent results, weaker host-rock generates a greater CMSU prior to failure onset. At a given depth, the variability in predicted CMSU and critical overpressure significantly decreases when Young's modulus is greater than 40 GPa, suggesting that host-rock deformation is no longer sensitive to Young's modulus once the host-rock is strong enough (Fig. 3). The models with different Poisson's ratio from 0.15 to 0.35 have similar CMSUs and critical overpressures before failure onset (Fig. 3). Therefore, the brittle failure of the magma chamber is much more sensitive to Young's modulus than to Poisson's ratio. Like Poisson's ratio, the internal friction angle has less effect on the CMSU before brittle failure for stiffer host-rocks (Fig. 4), especially when the chamber is deep. However, for the soft host-rock (E = 5 GPa), the variation in CMSU or overpressure due to the internal friction angle is still large even for a deep chamber, indicating an accurate estimation in rock properties for weak host-rock is crucial to failure prediction (Fig. 4).

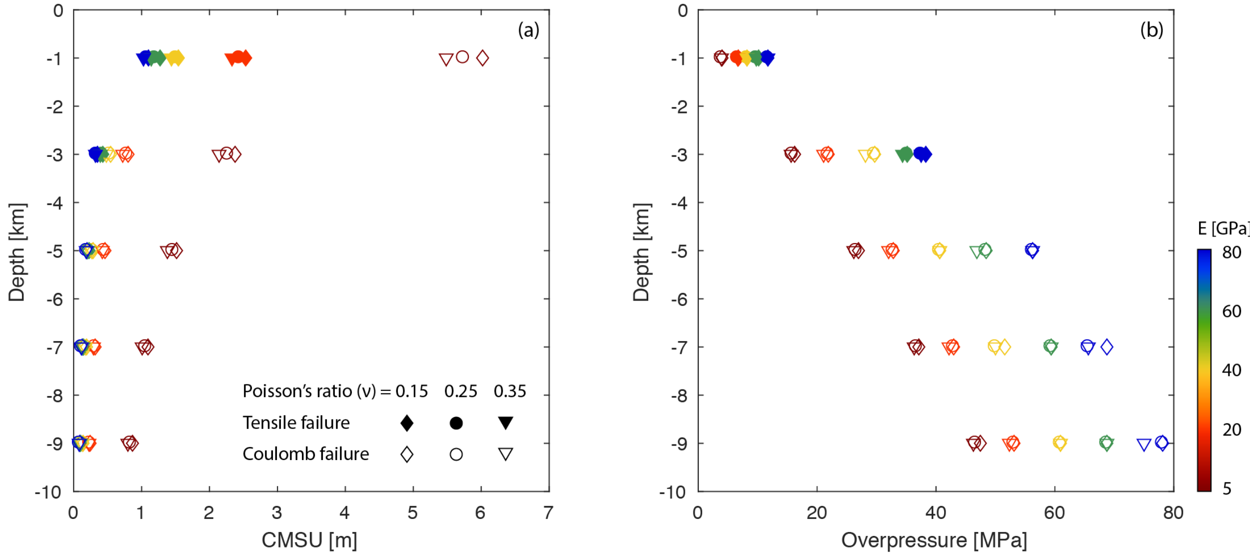

Figure 3. The effects of Young's modulus and Poisson's ratio on brittle failure with variations in the source depth to center (Elastic Test 1). A constant internal friction angle (φ = 25°) is assumed. (a) The Critical Maximum Surface Uplift (CMSU) for models with different magma chamber depths. The CMSU is the maximum value of the surface uplift that can be observed before any failure is initiated around the magma chamber. (b) The corresponding overpressures of the magma chamber when failure occurs. The shape of the marker indicates the Poisson's ratio of the model. The filled or open marker shows the case that the initial failure is tensile or Coulomb, respectively, same as Figs 4-6. The color represents the assumed Young's Modulus of the host, rock same as Figs 4-6.

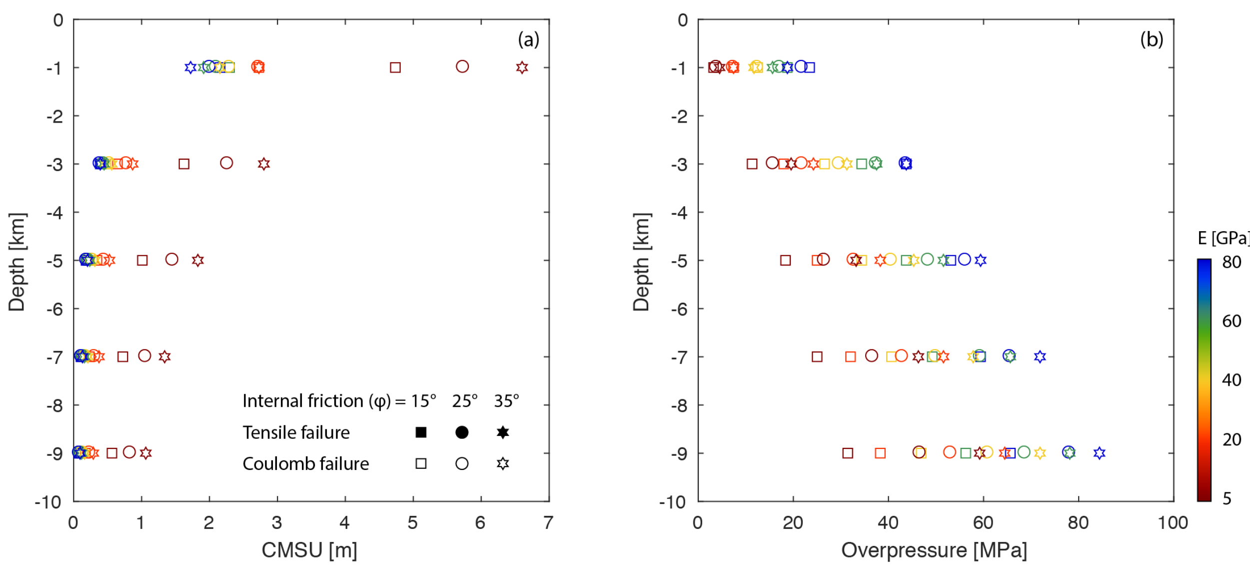

Figure 4. The effects of Young's modulus and internal friction angle on Coulomb failure with variations in the source depth to center (Elastic Test 1). A constant Poisson's ratio (ν = 0.25) is assumed. (a) The Critical Maximum Surface Uplift (CMSU) for models with different sizes of

magma chamber. (b) The corresponding overpressures of the magma chamber when failure occurs. The shape of the marker indicates the internal friction angle of the model.

For the chambers located at the same depth (Elastic Test 2), smaller chambers fail with lower CMSUs due to the higher overpressures needed to generate surface deformation (Fig. 5a). The size of the chamber also magnifies the range of the CMSU caused by the Young's modulus, suggesting that the behavior of large magmatic systems is strongly dependent on rock properties whereas smaller chambers ($R_1 < 1$ km) may be less sensitive (Fig. 5a). The overarching control on failure onset appears to be overpressure. Regardless of the assumed chamber geometry, the overpressure magnitude is similar at the moment of failure onset for a given Young's modulus (Fig. 5b). All of the models in Elastic Test 2 have the same magma chamber aspect ratio (R_1/R_2), which leads to the same pattern of near-field stress concentration regardless of the scales of the model. Like Elastic Test 1, the Poisson's ratio (Fig. 5) and internal friction angle (Fig. S6a and b) has little impact on the brittle failure.

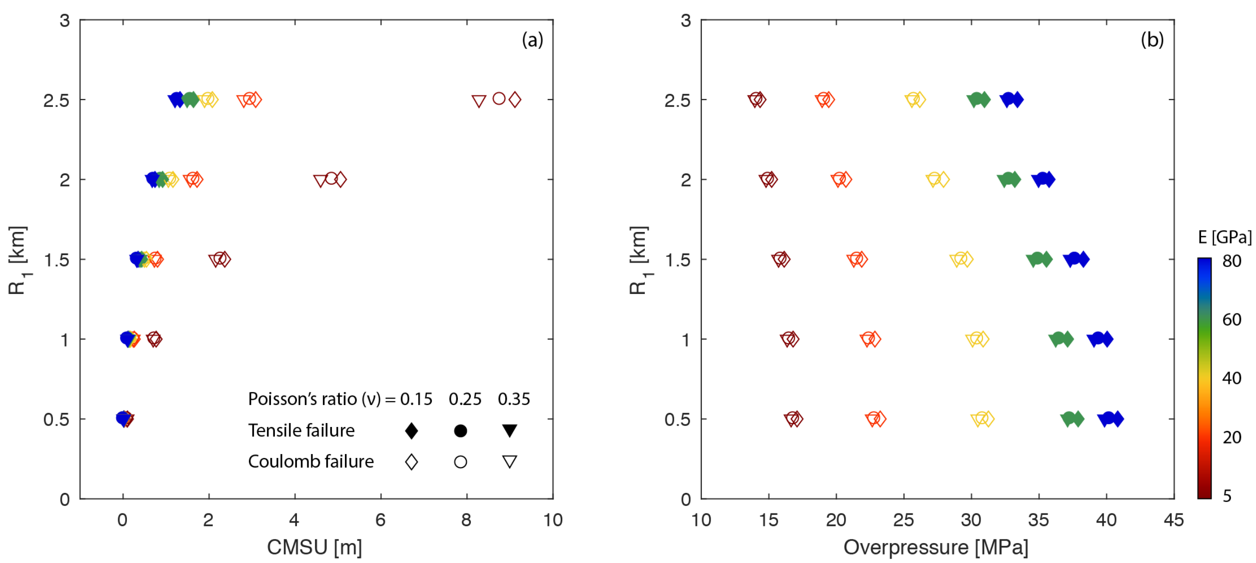

Figure 5. The effects of Young's modulus and Poisson's ratio on brittle failure with variations in the chamber size as described by the half-width (Elastic Test 2). A constant internal friction angle (φ = 25°) is assumed. (a) The Critical Maximum Surface Uplift (CMSU) for models with different size of magma chamber. R_1 is the length of the long axis of the magma chamber, which is three times longer than the short axis. (b) The corresponding overpressures of the magma chamber when failure occurs. The shape of the marker indicates the Poisson's ratio of the model.

In Elastic Test 1, larger overpressures are necessary for deeper chambers to create the same amount of surface uplift, while the overpressure and size of the chamber is not distinguishable in Elastic Test 2. A deep magma chamber can also generate the same magnitude of surface uplift as the shallower chambers by enlarging the chamber instead of accumulating overpressure, but the wavelength will vary (Fig. S7; Elastic Test 3). Unlike Elastic Test 1, a deep and large chamber creates larger CMSU than a shallow and small chamber (Fig. S7c). The range of the CMSU also increases with increasing depth and size. A greater overpressure is needed to initiate failure in models with deeper and larger chambers, simply due to higher confining pressure (Fig. S7d).

The aspect ratio of an oblate spheroidal chamber with the same volume has less impact on the CMSU than the depth and radius (Elastic Test 4; Fig. 6a). A prolate (conduit-like) chamber has lower CMSU at failure, and its aspect ratio has far less effects on the CMSU compared to an oblate chamber. When the magma body is sill-like, the CMSU decrease slightly with growing aspect ratio. The CMSU is much less sensitive to aspect ratios than to depth (Fig. 3 and 4) and radius (Fig. 5) at least for oblate chambers. However, the variability of the overpressures required to initiate failure is quite large (Fig. 6b). A highly-oblate chamber ($R_1/R_2 = 5$) requires less than 25 MPa to initiate failure, while this value rises to 150 MPa for a spherical chamber whose aspect ratio is one (Fig. 6b). The critical overpressure falls back to 40 MPa when the chamber becomes prolate. Notably, the extremely high overpressure for the spherical chamber does not create a significant uplift, suggesting the stability of the whole system is sensitive to aspect ratio. Although a perfectly spherical chamber has the greatest stability, it is unlikely to exist in natural settings.

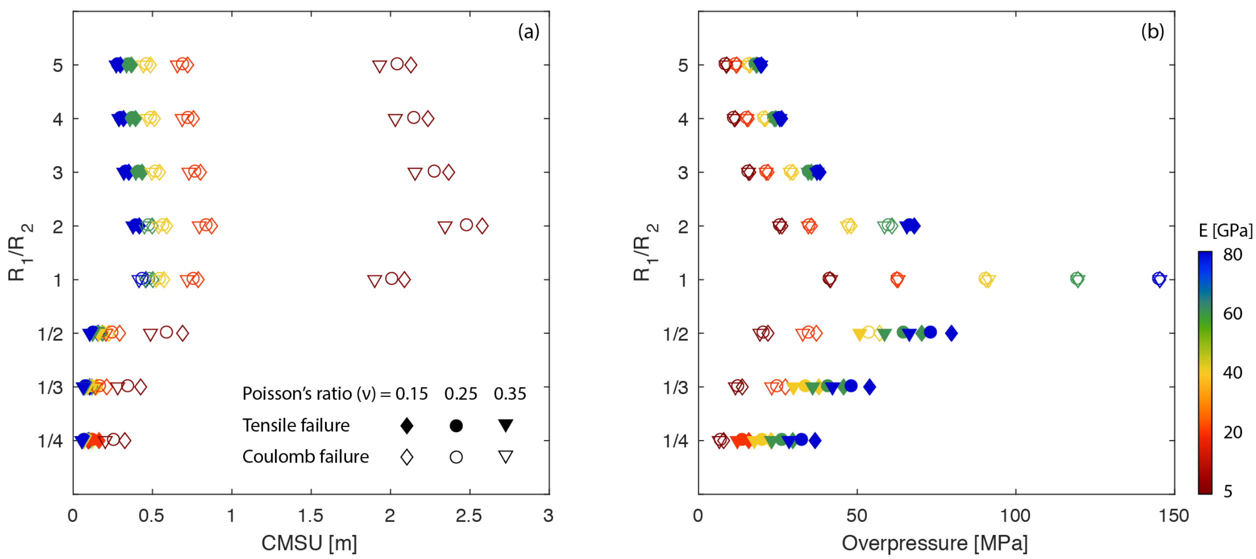

Figure 6. The effects of Young's modulus and Poisson's ratio on brittle failure with variations in the chamber aspect ratio (Elastic Test 4). A constant internal friction angle ($\varphi = 25°$) is assumed. (a) The Critical Maximum Surface Uplift (CMSU) for models with different shapes of the magma chamber. The sensitivity of the CMSU to the aspect ratio is noticeably decreased when the magma body is conduit-like ($R_1/R_2 < 1$). (b) The corresponding overpressures of the magma chamber when failure occurs. The shape of the marker indicates the Poisson's ratio of the model.

In all elastic tests (Figs. 3-6), Young's modulus shows the most significant effect on the development of brittle failure. The stiffer (Young's modulus > 40 GPa) and stronger ($C_0 > 40$ MPa and $T_0 > 16$ MPa) the host-rock (e.g., intact granite, diorite, and metamorphic rocks; Perras & Diederichs, 2014) is assumed to be, the more likely that tensile failure will initiate around the chamber boundary first, while models with a weak host rock favor Coulomb failure at the chamber wall. Because a higher cohesion is expected in stronger rocks, making their Coulomb failure envelope more difficult to reach (Fig. 7). Additionally, deeper chambers prefer Coulomb failure as the first failure onset, since tensile failure is harder to initiate due to the high confining pressure at depth.

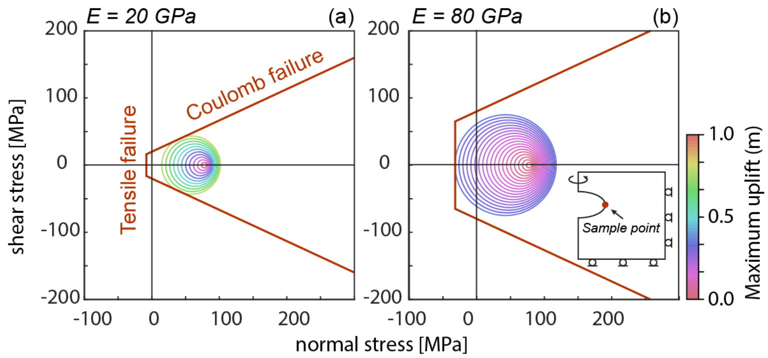

Figure 7. Mohr circle diagrams illustrating that the initial failure type is controlled by host-rock stiffness and strength. The Mohr circles represent of the stress state at the tip of the chamber in Model Dp2 (Table 2; Depth = 3 km, R_1 = 1.5 km, and R_2 = 0.5 km) as shown in the inserted plot. (a) For the host-rock with relatively low Young's Modulus (E = 20 GPa) and cohesion (20 MPa), the Mohr circle increases and touches the Coulomb failure envelop first. (b) The high cohesion (80 MPa) of the stronger rock (E = 80 GPa) allows the Mohr circle to reach tensile failure first.

Although laboratory rock tests indicate that tensile strength of rocks ranges from ~1 to ~20 MPa, in natural conditions, the host-rock may be fractured, causing its tensile strength greatly decreased. We compare the CMSU and critical overpressure of the models assuming T_0 = E /2500 to the models with T_0 = 0 (Fig. S8). The results show that using zero tensile strength makes slightly lower CMSU at tensile failure onset, indicating CMSU is not sensitive to tensile strength (Fig. S8). The critical overpressure of the models with T_0 = 0 is constant for each model with the same geometry but different Young's modulus, indicating that the critical overpressure for tensile failure is independent of Young's modulus.

4 Discussion

4.1 Uncertainty derived from rock properties

The results of the viscoelastic tests indicate that the overpressure at failure onset is independent of the viscosity of the host-rock (Fig. S4) and is only determined by its elastic moduli. A higher overpressure is needed to trigger failure in a stiffer and stronger system (Fig. S4 and Fig. 3-6). Whether or not the viscosity of the host-rock will impact the brittle failure forecast is determined by viscoelastic relaxation time of the crust (Fig. 2). The CMSU at failure onset for a particular elastic model will be lower than the viscous model with the same elastic moduli, only if the time scale of the pressurization episode is longer than the viscous relaxation time. Therefore, knowing the relaxation time of the system as well as the over-pressurizing rate is useful to determine if the model needs to take viscosity into consideration. Models with higher viscosities and lower Young's moduli have longer relaxation times. For a cold crust with a viscosity larger than 10^{20} $Pa \cdot s$, an elastic model is sufficient to simulate the deformation and failure if the replenishment prior to the failure is < 100 years. For a quartz-bearing crust at 350°C (Newman et al., 2001), the crust will still behave elastically if the replenishment episode lasts no more than several years. For a rhyolite close to the solidus, the viscous effect cannot be neglected if it takes more than one day to build overpressure to fail the host-rock (Fig. 2). The overpressures required for all viscoelastic models to initiate failure along the chamber wall are the same as the elastic models with the same elastic moduli (Fig. S4), since the brittle failure of the rocks is only controlled by its strength and current stress state.

Among Young's modulus, Poisson's ratio, internal friction angle and tensile strength, Young's modulus plays the most important role in the displacement at brittle failure onset. All tests conducted indicate that a lower Young's modulus results in greater surface deformation (i.e., CMSU) before the host-rock starts to fail, even if the host-rock has lower compressive and tensile strengths (Fig. 3-6). The difference in CMSU between the stiffest and weakest rocks is largely dependent on the location and geometry of the magma body. This difference can be as great as several meters if the magma body is large and shallow (Fig. 3a and 5a). The accuracy of the failure forecast for a system with a low Young's modulus is tenuous without constraining the elastic properties. However, the sensitivity of the CMSU to Young's modulus decreases with increasing Young's modulus, especially when assuming a proportional rock strength (Aggistalis et al., 1996; Dinçer et al., 2004). The elastic properties of the host-rock are determined by the composition and depth. Generally, the Young's modulus of the upper crust increases with depth from ~10 GPa at the surface to ~50 GPa around 2~3 km, and up to ~100 GPa below 5~6 km (e.g., Gudmundsson, 1988). The uncertainty of Poisson's ratio does not significantly impact the CMSU (Fig. 3, 5, and 6). Poisson's ratio of the upper crust is more well constrained than Young's modulus (Christensen, 1996). A poor constraint on internal friction angle will introduce large uncertainties when the Young's modulus is < 5 GPa (Fig. 4). Therefore, if the magma body is near the surface or in the volcanic edifice, where the Young's modulus is low, the uncertainty in its material properties will be problematic for forecasting failure initiation. This limitation may be overcome by conducting rock tests on samples from the volcano, since the near surface samples may represent the host-rock for a shallow magma body. But laboratory test results can only be scaled up to represent in-situ/outcrop scale host-rocks, if the host-rock is not strongly fractured. On the other hand, for a deep magma body, the uncertainty introduced by elastic moduli is negligible compared to the uncertainties derived from other factors such as depth (Fig. 3) and radius (Fig. 4).

4.2 Geometrical considerations for geodetic observations

The magnitude of the surface deformation before the onset of host-rock failure (CMSU) is strongly affected by the depth (Fig. 3 and 4), size (Fig. 5), and shape (Fig. 6) of the magma body. Under the same overpressure, a deep, small, or prolate magma chamber is limited in the magnitude of vertical surface displacement it can promote before its failure. For example, the conduit inflation of Colima volcano created only ~4 cm uplift no earlier than 11 days prior to the 2013 explosive eruption (Salzer et al., 2014). While, an oblate source under Sierra Negra volcano, Galápagos created ~5 m vertical displacement from 1992 until its 2005 eruption (Chadwick et al., 2006). Beside the absolute magnitude of vertical displacement, the rate of displacement is also important. For volcanoes with small CMSUs, slow deformation rates can ensure their precursory deformation being captured by weekly or monthly geodetic measurement such as InSAR (e.g., Lohman & Simons, 2005; Pinel et al., 2014).

Among all of the geometric uncertainties, the error introduced by the inaccurate estimation of a magma system's size has the greatest effect on producing a failure forecast. Unlike depth and aspect ratio, size and overpressure of a magma body can hardly be distinguished from one another by geodetic observations alone (e.g., Mogi, 1958). Therefore, additional constraints on the dimensions of the magma plumbing system are necessary, such as seismic tomography, gravity, and/or magnetotellurics.

4.3 Failure and VT-earthquakes

Volcano-Tectonic (VT) earthquakes can be triggered by the brittle failure of the host-rock. A combination of seismicity and geodesy gives insight into both stress field and deformation field which increases the accuracy of forecasting volcanic unrest (e.g., Lengliné et al., 2008, Carrier et al., 2015). Our models show that, when the overpressure of the magma chamber increases gradually, stronger host-rock favors the initiation tensile failure (Fig. 8), while weaker host-rock favors Coulomb failure and the generation of shear fractures first. In the weak host rock case, more overpressure is needed to open tensional cracks for dikes, even though the occurrence of the shear fractures will greatly reduce the tensile strength of the rock (Fig. 7a). Therefore, during the period between Coulomb failure onset and tensile failure onset, the earthquake swarms are only generated by shear fractures, indicating that seismicity should be dominated by high-frequency (VT) events. Once tensile failure is initiated, it is very likely followed by dike propagation and possible eruption (White & McCausland, 2016). During dike propagation, earthquakes can be triggered by both brittle failure of host-rocks (Roman & Cashman, 2006), and magma/volatile movement in the dike, indicating low-frequency earthquakes may be observed (McNutt, 2005). Since Coulomb failure does not open a pathway for magma to move to the surface, volcanoes triggering Coulomb failure first may experience a longer period of seismic unrest until tensile failure is initiated. The numerical results show that shallow magma chambers surrounded by stronger host-rock favor tensile failure as their initial failure type, indicating those systems are likely to erupt without triggering a lot of VT earthquakes, if the speed of dike propagation is fast enough. For example, the 2008 Okmok eruption was preceded by less than 5 hours of seismicity (Larsen et al., 2009), which may be related with dike propagation after tensile failure initiated.

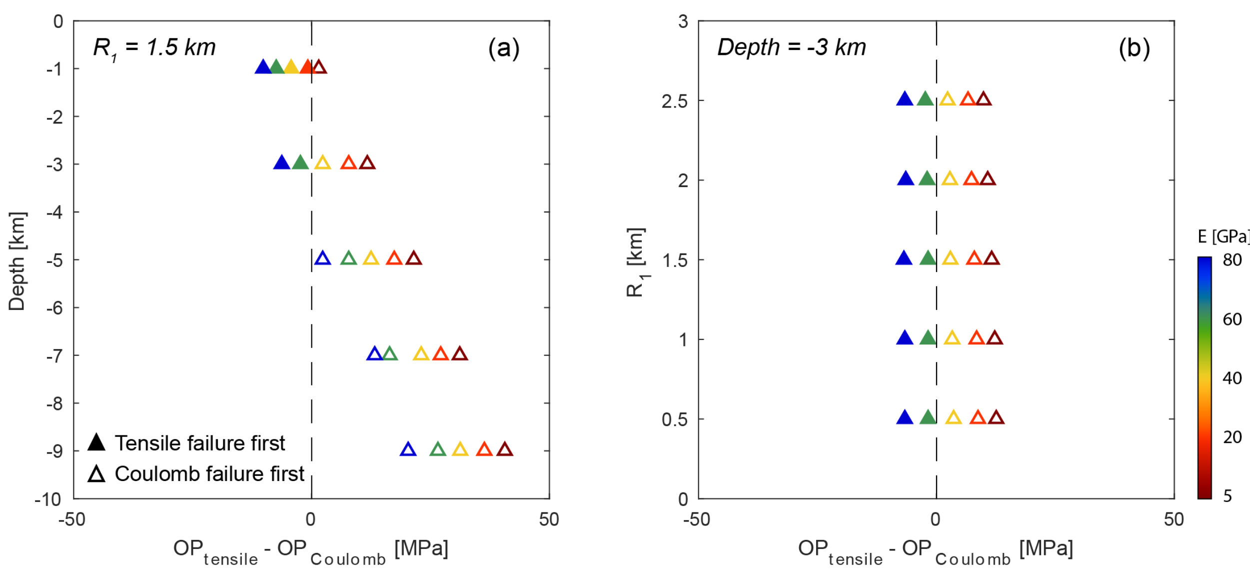

Figure 8. The overpressure required to initiate tensile failure compared to the overpressure required to initiate Coulomb failure ($OP_{Tensile} – OP_{Coulomb}$) for models with different chamber

depths (a) and half-widths (b). (a) and (b) show the results from models with internal friction = 25° and Poisson's ration = 0.25 in Elastic Test 1 and Elastic Test 2. If the difference in overpressure for the two types of failure is positive, tensile failure will occur after Coulomb failure is triggered. In this case, it is expected that shear fractures will develop generating earthquake swarms during a relatively long period prior to the onset of tensile failure and magma propagation. On the other hand, if the difference in overpressure is negative, Coulomb failure will not be triggered prior to dike propagation.

4.4 Limitations

Forecasting eruptions by modeling failure as an instantaneous response to the host rock stress state has three main limitations. First, the relationship between failure and eruptions is unclear. Through-going failure which connects the magma chamber to the surface has been indicated as a potential catalyst of caldera formation eruptions (e.g., Gregg et al., 2012, 2013; Cabaniss et al., 2018). However, large caldera eruption cycles may be much longer than thousands of years, far outside of the time scales in this investigation. When forecasting eruptions of a system with much shorter eruption cycles, the effect of diking events cannot be neglected. Dikes may be solidified and trapped depending on their temperature and viscosity (e.g., Delaney & Pollard, 1982; Rubin, 1995; Maccaferri et al., 2011), laying huge uncertainties between failure initiations and the ability of magma to propagate to the surface and erupt. The second shortcoming in the current models is the lack of changes in the rock properties due to failure accumulation. In this study, we focus on the initiation of the failure controlled by the pre-failure stress state, which is more predictable than the stress state evolution during failure propagation. Failure introduces localization of weakness in the host-rock and is usually anisotropic (e.g., Heap et al., 2010). The first two limitations may be overcome by applying dynamic failure propagation models, which are widely used in hydrofracturing studies (e.g., Camacho & Ortiz, 1996; Fu et al., 2013). However, numerical models of dike propagation may be more complicated than hydrofracturing due to the multiphase nature of propagating magma. Another limitation is the use of homogeneous rock properties, since rock properties vary with depth and temperature, and are also affected by pre-existing structures. A final limitation of these models, which is also fundamental to most volcano modeling approaches, is the lack of knowledge of the initial state. In the presented approach, it is assumed that there is no stress accumulation prior to the observed inflation of the magma chamber. The assumption of an intact host-rock in equilibrium before precursory deformation may greatly impact model forecasts in many systems. Studying multiple volcanic eruption cycles may help to eliminate the effect of the unknown initial state. Furthermore, healing of the host-rock is another important factor, especially under the conditions such as high temperature, confining pressure, and repeated loading (e.g., Batzle et al., 1980; Fredrich & Wong, 1986; Smith et al., 2009). Future efforts should focus particular care to evaluate the impact of the pre-deformation stress condition on forecasts of system unrest and eruption potential.

5 Conclusion

A suite of numerical experiments was implemented to answer what is the effect of variations in rock properties on modeled overpressure and critical maximum surface uplift (CMSU) at failure onset along the wall of magma chambers. Model results indicate that, in most of cases, the predicted overpressure and CMSU at failure onset is sensitive to rock properties, which means without knowing rock properties can impair the accuracy of failure modeling.

The overpressure of the magma chamber at failure onset is affected by the elastic properties and strength of the host-rock. Neglecting the viscous effect results in lower CMSU predictions than the calculated CMSU if the time scale of pressurization is longer than the relaxation time of the crust. The CMSU before failure onset is much more sensitive to Young's modulus than to Poisson's ratio or internal friction angle, especially when the Young's modulus of the host-rock is < 20 GPa. The accuracy of host-rock stability estimates for a deep (> 5 km), small (half-width < 1 km) or prolate magma chamber are less likely to be impaired by the uncertainty from rock properties than by other uncertainties such as geometry. To forecast the unrest of small and/or prolate magma systems, frequent observations are necessary to record the subtle, and often rapid, precursory deformation prior to eruption. However, for shallow, large, or sill-like magma bodies, significant surface deformation may be observed prior to host rock failure initiation. Magma chambers surrounded by a weak host-rock (Young's modulus < 20 GPa) will continue to inflate after triggering Coulomb failure until tensile failure is initiated and dike propagation can be catalyzed. Therefore, prolonged earthquake swarms associated with Coulomb failure may be observed, providing extra information for eruption forecast.

Acknowledgement

We are grateful for helpful discussions with D. Roman, H. Le Mével, Z. Lu, M. Poland, R. Bendick, M. Coombs, J. Freymueller, J. Albright, H. Cabaniss, R. Goldman, V. Romano, and the UIUC Geodynamics Group. We would also like to thank J. Hickey, Y. Aoki, and two anonymous reviewers for their comments which greatly improved our manuscript. Research reported in this publication is supported by grants from NASA (19-EARTH19R-0104 – Zhan, 18-ESI18-0002 – Gregg) and the National Science Foundation (OCE 1834843, EAR 1752477 – Gregg). Model implementations presented here are available at GitHub (https://github.com/geoyanzhan3/JGR2019_RockProperty).

Reference

Aggistalis, G., Alivizatos, A., Stamoulis, D., & Stournaras, G. (1996). Correlating uniaxial compressive strength with schmidt hardness, point load index, Young's modulus, and mineralogy of gabbros and basalts (northern Greece). Bulletin of the International Association of Engineering Geology - Bulletin de l'Association Internationale de Géologie de l'Ingénieur, 54(1), 3–11. https://doi.org/10.1007/BF02600693

Albino, F., Pinel, V., & Sigmundsson, F. (2010). Influence of surface load variations on eruption likelihood: application to two Icelandic subglacial volcanoes, Grímsvötn and Katla. Geophysical Journal International, 181(3), 1510–1524. https://doi.org/10.1111/j.1365-246X.2010.04603.x

Albright, J. A., P. M. Gregg, Z. Lu, and J. Freymueller (2019), Hindcasting magma reservoir stability preceding the 2008 eruption of Okmok, Alaska, Geophysical Research Letters, https://doi.org/10.1029/2019GL083395.

Bato, M. G., Pinel, V., & Yan, Y. (2017). Assimilation of Deformation Data for Eruption Forecasting: Potentiality Assessment Based on Synthetic Cases. Frontiers in Earth Science, 5. https://doi.org/10.3389/feart.2017.00048

Bato, M. G., Pinel, V., Yan, Y., Jouanne, F., & Vandemeulebrouck, J. (2018). Possible deep connection between volcanic systems evidenced by sequential assimilation of geodetic data. Scientific Reports, 8(1), 11702. https://doi.org/10.1038/s41598-018-29811-x

Batzle, M. L., Simmons, G., & Siegfried, R. W. (1980). Microcrack closure in rocks under stress: Direct observation. Journal of Geophysical Research, 85(B12), 7072. https://doi.org/10.1029/JB085iB12p07072

Beauducel, F., Cornet, F.-H., Suhanto, E., Duquesnoy, T., & Kasser, M. (2000). Constraints on magma flux from displacements data at Merapi volcano, Java, Indonesia. Journal of Geophysical Research: Solid Earth, 105(B4), 8193–8203. https://doi.org/10.1029/1999JB900368

Biggs, J., Ebmeier, S. K., Aspinall, W. P., Lu, Z., Pritchard, M. E., Sparks, R. S. J., & Mather, T. A. (2014). Global link between deformation and volcanic eruption quantified by satellite imagery. Nature Communications, 5. http://www.nature.com/ncomms/2014/140403/ncomms4471/full/ncomms4471.html?message-global=remove

Biggs, Juliet, & Pritchard, M. E. (2017). Global Volcano Monitoring: What Does It Mean When Volcanoes Deform? Elements, 13(1), 17–22. https://doi.org/10.2113/gselements.13.1.17

Bradford, I. D. R., Fuller, J., Thompson, P. J., & Walsgrove, T. R. (1998). Benefits of assessing the solids production risk in a North Sea reservoir using elastoplastic modelling. In SPE/ISRM Rock Mechanics in Petroleum Engineering. Society of Petroleum Engineers.

Byerlee, J. D. (1978). Rock Friction and Earthquake Prediction, 414.

Cabaniss, H. E., Gregg, P. M., & Grosfils, E. B. (2018). The Role of Tectonic Stress in Triggering Large Silicic Caldera Eruptions. Geophysical Research Letters, 45(9), 3889–3895. https://doi.org/10.1029/2018GL077393

Camacho, G. T., & Ortiz, M. (1996). Computational modelling of impact damage in brittle materials. International Journal of Solids and Structures, 33(20–22), 2899–2938. https://doi.org/10.1016/0020-7683(95)00255-3

Carrier, A., Got, J.-L., Peltier, A., Ferrazzini, V., Staudacher, T., Kowalski, P., & Boissier, P. (2015). A damage model for volcanic edifices: Implications for edifice strength, magma pressure, and eruptive processes. Journal of Geophysical Research: Solid Earth, 120(1), 567–583. https://doi.org/10.1002/2014JB011485

Chadwick, W. W., Geist, D. J., Jónsson, S., Poland, M., Johnson, D. J., & Meertens, C. M. (2006). A volcano bursting at the seams: Inflation, faulting, and eruption at Sierra Negra volcano, Galápagos. Geology, 34(12), 1025–1028. https://doi.org/10.1130/G22826A.1

Chang, C., Zoback, M. D., & Khaksar, A. (2006). Empirical relations between rock strength and physical properties in sedimentary rocks. Journal of Petroleum Science and Engineering, 51(3), 223–237. https://doi.org/10.1016/j.petrol.2006.01.003

Cheng, C. H., & Johnston, D. H. (1981). Dynamic and static moduli. Geophysical Research Letters, 8(1), 39–42. https://doi.org/10.1029/GL008i001p00039

Christensen, N. I. (1996). Poisson's ratio and crustal seismology. Journal of Geophysical Research: Solid Earth, 101(B2), 3139–3156. https://doi.org/10.1029/95JB03446

Currenti, G., Del Negro, C., & Ganci, G. (2007). Modelling of ground deformation and gravity fields using finite element method: an application to Etna volcano. Geophysical Journal International, 169(2), 775–786. https://doi.org/10.1111/j.1365-246X.2007.03380.x

De Natale, G., & Pingue, F. (1996). Ground Deformation Modeling in Volcanic Areas. In R. Scarpa & R. I. Tilling (Eds.), Monitoring and Mitigation of Volcano Hazards (pp. 365–388). Berlin, Heidelberg: Springer Berlin Heidelberg. https://doi.org/10.1007/978-3-642-80087-0_11

Del Negro, C., Currenti, G., & Scandura, D. (2009). Temperature-dependent viscoelastic modeling of ground deformation: application to Etna volcano during the 1993–1997 inflation period. Physics of the Earth and Planetary Interiors, 172(3), 299–309.

Delaney, P. T., & Pollard, D. D. (1982). Solidification of basaltic magma during flow in a dike. American Journal of Science, 282(6), 856–885. https://doi.org/10.2475/ajs.282.6.856

Dinçer, I., Acar, A., Çobanoğlu, I., & Uras, Y. (2004). Correlation between Schmidt hardness, uniaxial compressive strength and Young's modulus for andesites, basalts and tuffs. Bulletin of Engineering Geology and the Environment, 63(2), 141–148. https://doi.org/10.1007/s10064-004-0230-0

Fredrich, J. T., & Wong, T. (1986). Micromechanics of thermally induced cracking in three crustal rocks. Journal of Geophysical Research: Solid Earth, 91(B12), 12743–12764. https://doi.org/10.1029/JB091iB12p12743

Fu, P., Johnson, S. M., & Carrigan, C. R. (2013). An explicitly coupled hydro-geomechanical model for simulating hydraulic fracturing in arbitrary discrete fracture networks: FULLY COUPLED MODEL FOR HYDRO-FRACTURING IN ARBITRARY FRACTURE NETWORKS. International Journal for Numerical and Analytical Methods in Geomechanics, 37(14), 2278–2300. https://doi.org/10.1002/nag.2135

Gerbault, M., Cappa, F., & Hassani, R. (2012). Elasto-plastic and hydromechanical models of failure around an infinitely long magma chamber. Geochemistry, Geophysics, Geosystems, 13(3). https://doi.org/10.1029/2011GC003917

Gerbault, M., Hassani, R., Lizama, C. N., & Souche, A. (2018). Three-Dimensional Failure Patterns Around an Inflating Magmatic Chamber. Geochemistry, Geophysics, Geosystems, 19(3), 749–771. https://doi.org/10.1002/2017GC007174

Gercek, H. (2007). Poisson's ratio values for rocks. International Journal of Rock Mechanics and Mining Sciences, 44(1), 1–13. https://doi.org/10.1016/j.ijrmms.2006.04.011

Grapenthin, R., Sigmundsson, F., Geirsson, H., Árnadóttir, T., & Pinel, V. (2006). Icelandic rhythmics: Annual modulation of land elevation and plate spreading by snow load. Geophysical Research Letters, 33(24). https://doi.org/10.1029/2006GL028081

Gregg, P. M., Mével, H. L., Zhan, Y., Dufek, J., Geist, D., & Chadwick, W. W. (2018). Stress triggering of the 2005 eruption of Sierra Negra volcano, Galápagos. Geophysical Research Letters. https://doi.org/10.1029/2018GL080393

Gregg, Patricia M., & Pettijohn, J. C. (2016). A multi-data stream assimilation framework for the assessment of volcanic unrest. Journal of Volcanology and Geothermal Research, 309, 63–77. https://doi.org/10.1016/j.jvolgeores.2015.11.008

Gregg, P.M., de Silva, S. L., Grosfils, E. B., & Parmigiani, J. P. (2012). Catastrophic caldera-forming eruptions: Thermomechanics and implications for eruption triggering and maximum caldera dimensions on Earth. Journal of Volcanology and Geothermal Research, 241–242, 1–12. https://doi.org/10.1016/j.jvolgeores.2012.06.009

Gregg, P.M., de Silva, S. L., & Grosfils, E. B. (2013). Thermomechanics of shallow magma chamber pressurization: Implications for the assessment of ground deformation data at active volcanoes. Earth and Planetary Science Letters, 384, 100–108. https://doi.org/10.1016/j.epsl.2013.09.040

Grosfils, E. B., McGovern, P. J., Gregg, P. M., Galgana, G. A., Hurwitz, D. M., Long, S. M., & Chestler, S. R. (2015). Elastic models of magma reservoir mechanics: a key tool for investigating planetary volcanism. In T. Platz, M. Massironi, P. K. Byrne, & H. Hiesinger (Eds.), Volcanism and Tectonism Across the Inner Solar System (Vol. 401, pp. 239–267). Bath: Geological Soc Publishing House.

Gudmundsson, A. (1988). Effect of tensile stress concentration around magma chambers on intrusion and extrusion frequencies. Journal of Volcanology and Geothermal Research, 35(3), 179–194. https://doi.org/10.1016/0377-0273(88)90015-7

Heap, M. J., Faulkner, D. R., Meredith, P. G., & Vinciguerra, S. (2010). Elastic moduli evolution and accompanying stress changes with increasing crack damage: implications for stress changes around fault zones and volcanoes during deformation: Elastic moduli evolution and stress changes. Geophysical Journal International, 183(1), 225–236. https://doi.org/10.1111/j.1365-246X.2010.04726.x

Hickey, J., & Gottsmann, J. (2014). Benchmarking and developing numerical Finite Element models of volcanic deformation. Journal of Volcanology and Geothermal Research, 280, 126–130. https://doi.org/10.1016/j.jvolgeores.2014.05.011

Hickey, J., Gottsmann, J., & Mothes, P. (2015). Estimating volcanic deformation source parameters with a finite element inversion: The 2001-2002 unrest at Cotopaxi volcano, Ecuador. Journal of Geophysical Research: Solid Earth, 120(3), 1473–1486. https://doi.org/10.1002/2014JB011731

Jaeger, J. C., Cook, N. G. W., & Zimmerman, R. W. (2007). Fundamentals of rock mechanics (4th ed). Malden, MA: Blackwell Pub.

Larsen, J., Neal, C., Webley, P., Freymueller, J., Haney, M., McNutt, S., et al. (2009). Eruption of Alaska Volcano Breaks Historic Pattern. Eos, Transactions American Geophysical Union, 90(20), 173. https://doi.org/10.1029/2009EO200001

Lengliné, O., Marsan, D., Got, J.-L., Pinel, V., Ferrazzini, V., & Okubo, P. G. (2008). Seismicity and deformation induced by magma accumulation at three basaltic volcanoes. Journal of Geophysical Research: Solid Earth, 113(B12). https://doi.org/10.1029/2008JB005937

Lohman, R. B., & Simons, M. (2005). Some thoughts on the use of InSAR data to constrain models of surface deformation: Noise structure and data downsampling: THOUGHTS ON INSAR. Geochemistry, Geophysics, Geosystems, 6(1), n/a-n/a. https://doi.org/10.1029/2004GC000841

Maccaferri, F., Bonafede, M., & Rivalta, E. (2011). A quantitative study of the mechanisms governing dike propagation, dike arrest and sill formation. Journal of Volcanology and Geothermal Research, 208(1–2), 39–50. https://doi.org/10.1016/j.jvolgeores.2011.09.001

Masterlark, T. (2007). Magma intrusion and deformation predictions: Sensitivities to the Mogi assumptions. Journal of Geophysical Research, 112(B6). https://doi.org/10.1029/2006JB004860

McNutt, S. R. (2005). Volcanic Seismology. Annual Review of Earth and Planetary Sciences, 33, 461–491. https://doi.org/10.1146/annurev.earth.33.092203.122459

Mogi, K. (1958). Relations between the eruptions of various volcanoes and the deformations of the ground surfaces around them. Bull. Earthq. Res. Inst., University of Tokyo, 36, 99–134.

Newman, A. V., Dixon, T. H., Ofoegbu, G. I., & Dixon, J. E. (2001). Geodetic and seismic constraints on recent activity at Long Valley Caldera, California: evidence for viscoelastic rheology. Journal of Volcanology and Geothermal Research, 105(3), 183–206.

Perras, M. A., & Diederichs, M. S. (2014). A Review of the Tensile Strength of Rock: Concepts and Testing. Geotechnical and Geological Engineering, 32(2), 525–546. https://doi.org/10.1007/s10706-014-9732-0

Pinel, V., Poland, M. P., & Hooper, A. (2014). Volcanology: Lessons learned from Synthetic Aperture Radar imagery. Journal of Volcanology and Geothermal Research, 289, 81–113. https://doi.org/10.1016/j.jvolgeores.2014.10.010

Roman, D. C., & Cashman, K. V. (2006). The origin of volcano-tectonic earthquake swarms. Geology, 34(6), 457. https://doi.org/10.1130/G22269.1

Rubin, A. M. (1995). Propagation of Magma-Filled Cracks. Annual Review of Earth and Planetary Sciences, 23(1), 287–336. https://doi.org/10.1146/annurev.ea.23.050195.001443

Salzer, J. T., Nikkhoo, M., Walter, T. R., Sudhaus, H., Reyes-DÃ¡vila, G., BretÃ³n, M., & ArÃ¡mbula, R. (2014). Satellite radar data reveal short-term pre-explosive displacements and a complex conduit system at VolcÃ¡n de Colima, Mexico. Frontiers in Earth Science, 2. https://doi.org/10.3389/feart.2014.00012

Segall, P. (2019). Magma chambers: what we can, and cannot, learn from volcano geodesy. Philosophical Transactions of the Royal Society A: Mathematical, Physical and Engineering Sciences, 377(2139), 20180158. https://doi.org/10.1098/rsta.2018.0158

Smith, R., Sammonds, P. R., & Kilburn, C. R. J. (2009). Fracturing of volcanic systems: Experimental insights into pre-eruptive conditions. Earth and Planetary Science Letters, 280(1–4), 211–219. https://doi.org/10.1016/j.epsl.2009.01.032

Sparks, R. S. J. (2003). Forecasting volcanic eruptions. Earth and Planetary Science Letters, 210(1–2), 1–15. https://doi.org/10.1016/S0012-821X(03)00124-9

White, R., & McCausland, W. (2016). Volcano-tectonic earthquakes: A new tool for estimating intrusive volumes and forecasting eruptions. Journal of Volcanology and Geothermal Research, 309, 139–155. https://doi.org/10.1016/j.jvolgeores.2015.10.020

Yang, X.-M., Davis, P. M., & Dieterich, J. H. (1988). Deformation from inflation of a dipping finite prolate spheroid in an elastic half-space as a model for volcanic stressing. Journal of Geophysical Research: Solid Earth, 93(B5), 4249–4257.

Zhan, Y., & Gregg, P. M. (2017). Data assimilation strategies for volcano geodesy. Journal of Volcanology and Geothermal Research, 344(Supplement C), 13–25. https://doi.org/10.1016/j.jvolgeores.2017.02.015

Zhan, Y., Gregg, P. M., Chaussard, E., & Aoki, Y. (2017). Sequential Assimilation of Volcanic Monitoring Data to Quantify Eruption Potential: Application to Kerinci Volcano, Sumatra. Frontiers in Earth Science, 5. https://doi.org/10.3389/feart.2017.00108